MOLECULAR AND CELLULAR BIOLOGY, Apr. 2001, p. 2880–2890 Vol. 21, No. 8
0270-7306/01/$04.00+0 DOI: 10.1128/MCB.21.8.2880–2890.2001

Requirement for the Murine Zinc Finger Protein ZFR in Perigastrulation Growth and Survival

MADELEINE J. MEAGHER† AND ROBERT E. BRAUN*

Department of Genetics, University of Washington, Seattle, Washington

Received 27 July 2000/Returned for modification 1 September 2000/Accepted 3 January 2001

The transition from preimplantation to postimplantation development leads to the initiation of complex cellular differentiation and morphogenetic movements, a dramatic decrease in cell cycle length, and a commensurate increase in the size of the embryo. Accompanying these changes is the need for the transfer of nutrients from the mother to the embryo and the elaboration of sophisticated genetic networks that monitor genomic integrity and the homeostatic control of cellular growth, differentiation, and programmed cell death. To determine the function of the murine zinc finger protein ZFR in these events, we generated mice carrying a null mutation in the gene encoding it. Homozygous mutant embryos form normal-appearing blastocysts that implant and initiate the process of gastrulation. Mutant embryos form mesoderm but they are delayed in their development and fail to form normal anterior embryonic structures. Loss of ZFR function leads to both an increase in programmed cell death and a decrease in mitotic index, especially in the region of the distal tip of the embryonic ectoderm. Mutant embryos also have an apparent reduction in apical vacuoles in the columnar visceral endoderm cells in the extraembryonic region. Together, these cellular phenotypes lead to a dramatic development delay and embryonic death by 8 to 9 days of gestation, which are independent of p53 function.

Gastrulation of the mammalian embryo initiates shortly after implantation into the maternal uterine tissue. The growing population of epiblast cells becomes the source for the generation of the definitive embryonic tissues: the mesoderm, endoderm, and ectoderm. Cell proliferation, differentiation, and morphogenetic movements all contribute to the establishment of the major body axes and the patterning of the definitive tissues (7).

Prior to implantation, embryonic cells divide very slowly, with little increase in mass. After implantation, as gastrulation initiates, a massive increase in growth occurs, accompanied by a decrease in cell cycle length (18). The number of ectodermal cells in particular rises from an estimated 120 cells at embryonic day 5.5 (E5.5) to 660 cells at E6.5 and 8,060 cells at E7.5. To accommodate this proliferation, the cell cycle length drops from approximately 11.5 h at E5.5 to 4.4 h at E6.5. In contrast, the newly formed mesodermal cells, first produced at E6.5, divide every 8 to 10 h.

The accelerated growth during gastrulation imposes increased biosynthetic and energy requirements on the embryo. A null mutation in the dihydrolipoamide dehydrogenase gene (*Dld*), which encodes an enzyme functioning in mitochondrial oxidative metabolism, results in developmental delay and lethality at this stage (8). The high proliferation rate of the epiblast also renders the cells more sensitive to metabolic inhibitors (12, 15). Furthermore, in comparison to trophoblasts, the epiblast cells are more vulnerable to damaging X-ray or UV irradiation (12).

The rapid mitotic division at gastrulation also places a stringent requirement on DNA surveillance systems. Several DNA repair and genome surveillance genes are expressed at gastrulation and are required for embryonic survival. In the absence of these regulators, instability in the genome accumulates and progression through the cell cycle slows or arrests, bringing development to a halt. This course of degeneration is observed in mouse embryos deficient for the DNA repair genes *Xrcc1* (20) and *Rad51* (9) and the tumor suppressor genes *Brca1* and *Brca2* (6, 10, 17, 19). Thus, the *Rad51, Brca1, Brca2* and *Xrcc1* genes together constitute a class of genes that functions at the cellular level in the maintenance of the integrity of the genome, and they are required for the progression of early postimplantation development.

The murine gene *Zfr* (zinc finger RNA binding) encodes a novel zinc finger protein that is expressed at high levels during gametogenesis (13). Conserved in *Drosophila melanogaster, Caenorhabditis elegans*, and *Homo sapiens, Zfr* encodes three widely spaced C_2H_2 zinc fingers followed by a 316-amino-acid domain, which is conserved among a small class of double-stranded RNA-binding proteins. This common feature in amino acid composition, together with the means by which *Zfr* was identified, suggests the gene encodes a zinc finger RNA-binding protein. However, results from Northwestern and Southwestern binding assays showed that recombinant ZFR protein has the capacity to bind both DNA and RNA in vitro (13). At this time, the nature of the ZFR substrates in vivo has not been identified. By Northern analysis, *Zfr* appears to be expressed at varying levels within all tissues. Within the testis and ovary, ZFR immunostaining is particularly strong in the nuclei of cells actively engaged in meiotic recombination. ZFR localizes to the meiotic chromosomes and is absent from interchromosomal regions. ZFR is also expressed in a subset of somatic cells within the gonads but is not detected in others.

The discovery of the unique motif organization within the ZFR amino acid sequence, in conjunction with the observed ZFR chromosome localization, led us to learn more about the functional properties of *Zfr* in the mouse. Through gene targeting in embryonic stem (ES) cells, a loss-of-function mutation in *Zfr* was cre-

* Corresponding author. Mailing address: Department of Genetics, Box 357360, 1959 NE Pacific, University of Washington, Seattle, WA 98195. Phone: (206) 543-1818. Fax: (206) 543-0754. E-mail: braun@u.washington.edu.

† Present address: Corixa Corporation, Seattle, WA 98104.

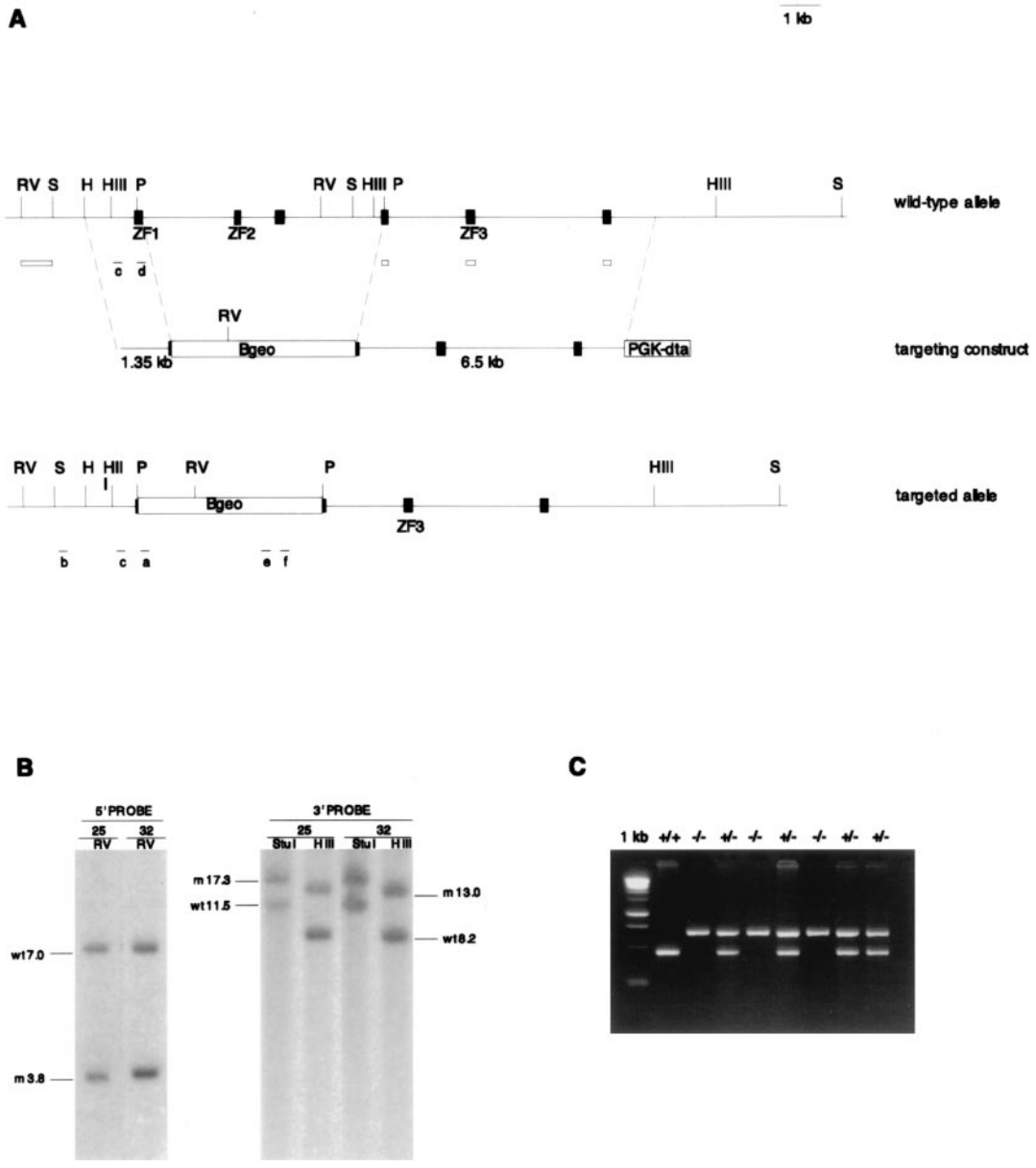

FIG. 1. (A) Gene targeting strategy, showing maps of the targeting construct and the wild-type and targeted alleles. Exons are shown as black boxes. Exons encoding zinc fingers 1, 2, or 3 are labeled ZF1, ZF2, or ZF3. The 5′ probe for Southern blotting is represented by the open box on the left. The 3′ probe sequences are represented by the three open boxes on the right. The PCR primers used for genotyping are designated a through f. A subset of restriction enzyme sites are shown. RV, *Eco*RV; S, *Stu*I; H, *Hpa*I; HIII, *Hin*dIII; P, *Pst*I. (B) Southern blots of ES cell DNA from clone 25 and clone 32 cut with *Eco*RV, *Stu*I, or *Hin*dIII. The 5′ probe detects the wild-type 7.0-kb and the mutant 3.8-kb *Eco*RV alleles. The 3′ probe detects the wild-type 11.5-kb and mutant 17.3-kb *Stu*I alleles and the wild-type 8.2-kb and mutant 13.0-kb *Hin*dIII alleles. (C) PCR products from E7.5 embryos, which were derived from a *Zfr* heterozygote intercross, electrophoresed on a 3% agarose gel. First lane, 1-kb DNA ladder (Life Technologies Gibco-BRL). PCR primers c and d detect the wild-type allele and generate a 377-bp band. Neo primers e and f generate a 660-bp band.

ated to investigate the requirement for *Zfr* in cell function and tissue development.

MATERIALS AND METHODS

Gene targeting *Zfr* locus in embryonic stem cells. A 129X1/SvJ mouse genomic bacteriophage library was screened with the *Sac*I-*Pst*I fragment (nucleotides 1215 to 1731) from cDNA *Zfr.1*. A 15-kb genomic clone was isolated, mapped, and used to generate a gene targeting construct (Fig. 1A). A 1.35-kb *Hpa*I-*Pst*I genomic fragment, containing exonic sequence at the 3′ end, was fused upstream of and in frame with a β*geo*-polyadenylation signal cassette that lacked the splice acceptor sequence. A 6-kb region from the 3′ end of the genomic clone constituted the right homologous arm. A cassette consisting of the polyglycerate kinase (*Pgk*) promoter, the diphtheria toxin (*dt*) gene, and a polyadenylation signal was cloned downstream of the right arm in the same orientation. The targeting construct DNA (25 μg) was linearized with *Sac*II and electroporated into 10^7 129X1/SvJ ES cells (Bio-Rad Gene Pulsar II, 500 μF, 0.24 kV). ES cells were cultured on a feeder layer of SNL cells in Dulbecco's modified Eagle's medium supplemented with 15% fetal bovine serum, glutamine, antibiotics, 0.1 mM β-mercaptomethanol, and 300 μg of G418 (Gibco BRL) per ml for 10 days (14). The plasmid bearing the β*geo* and *dt* cassettes, the AK7 ES cells, and the SNL cells were generously provided by P. Soriano. A fraction of each G418-resistant colony was picked with a drawn capillary tube for PCR

analysis. PCR was performed using a *Zfr* genomic primer that maps 5′ of the targeting construct's left arm (primer b, MM115: 5′ TCC ATA TGG TGG ACT CTC AG 3′), a primer to the 5′ end of β*geo* (primer a, 5βgeo2: 5′ GGG ATC CGC CAT GTC ACA G 3′), and Gittschier buffer PCR conditions (7). Twenty of 37 clones were positive for the 2.2-kb PCR product. DNA samples from six clones were prepared and digested with *Eco*RV, *Hin*dIII, or *Stu*I, electrophoresed on a 1% agarose gel, blotted, and probed three times (16). The template for the 5′ probe was the genomic *Eco*RV-*Stu*I fragment located 5′ of the left arm in the targeting construct. The template for the 3′ probe was PCR amplified with the *Zfr* cDNA sequence corresponding to the three exons in the right arm of the targeting construct. The *Neo* probe was a 660-bp PCR product from the β*geo* plasmid (primer e, neol: 5′ GAT TGC ACG CAG GTT CTC C 3′; and primer f, neo2: 5′ GTA GCC AAC GCT ATG TCC TG 3′). Five of the six lines were heterozygous at the *Zfr* locus and had no additional random integrations.

Generation of *Zfr* mutant mice. Cells from lines 25 and 32 were injected into day 3.5 C57BL/6 (Jackson Laboratories) blastocysts and implanted in DBA/BL6 pseudopregnant females. Germline-transmitting chimeric males, obtained from both lines, were backcrossed to C57BL/6 and 129S4/SvJae females. Progeny from all crosses were PCR genotyped using a wild-type allele-specific primer (primer d, MM105: 5′ CAG CTG ATC TTA CAA ACA TCA C 3′) with a primer to the left arm (primer c, MM112GR: 5′ CAA CAC CTG ACT GTC AAG TAA 3′) and targeted allele-specific neo primers e and f (listed above).

X-Gal staining of preimplantation embryos. Preimplantation embryos were flushed from the oviduct or uterine horns of pregnant females. Embryos were placed in 50-μl microdrops under oil. Embryos were washed in phosphate-buffered saline (PBS) plus 10 mg of bovine serum albumin/ml for 5 min, fixed in PBS plus 10 mg of bovine serum albumin/ml, 2% formaldehyde, and 0.2% glutaraldehyde for 10 min, and subsequently washed three times for 10 min. Embryos were stained in wash plus 2 mM $MgCl_2$, 5 mM ferricyanide, 5 mM ferrocyanide, and 1 mg of 5-bromo-4-chloro-3-indolyl-β-D-galactopyranoside (X-Gal) per ml.

Embryo dissections and histological analysis. Timed matings were conducted with F_1 *Zfr* heterozygous hybrid (129S4/SvJae × C57BL/6) mice. Females with copulation plugs the next day were considered to be at day 0.5 of gestation. Pregnant females were sacrificed at different time points of gestation, and the embryos were dissected free of maternal tissue, examined, photographed, and genotyped by PCR (see above). For histological preparations, embryos in decidua were fixed in methacarns (60% methanol, 30% chloroform, 10% glacial acetic acid) overnight at 4°C. Tissues were processed three times for 15 to 30 min in methanol, once for 45 to 60 min in methylbenzoate, twice for 20 to 30 min in xylenes, and twice for 20 to 45 min in paraffin. Incubation times depended on the sizes of the samples. Five-micrometer sections of tissues were cut from paraffin blocks. Sections were stained with hematoxylin and eosin.

Immunocytochemistry. Slides with paraffin sections were deparaffinized in xylenes and rehydrated. Slides were blocked in PBS plus 3% goat serum for 20 to 60 min. Anti-ZFR antibodies were diluted 1:500 in PBS with goat serum and incubated with sections at 4°C overnight. Sections were then washed in PBS three times for 5 min, incubated with 1:200 biotinylated goat anti-rabbit immunoglobulin G (Zymed, San Francisco, Calif.) for 30 min, washed, incubated with streptavidin-HRP (Zymed) for 15 min, and washed again. The aminoethylcarbazole color substrate was prepared according to instructions from Zymed and incubated for 5 to 15 min, followed by a 5-min rinse in tap water. Sections were mounted with Aquamount (Lerner Laboratories, Pittsburgh, Pa.).

BrdU labeling of embryos. Pregnant females at E6.5 were injected intraperitoneally with 100 μg of bromodeoxyuridine (BrdU) per gram of body weight and were sacrificed 1 h later. Decidua were removed, fixed in 4% paraformaldehyde overnight at 4°C, and processed as described previously (1). Five-micrometer sections were processed for anti-BrdU labeling. After deparaffinization, sections were incubated in 50% formamide–1× SSC–0.1% Tween (1× SSC is 0.15 M NaCl plus 0.015 M sodium citrate) at 70°C for 30 min, microwaved in 10 mM citric acid (pH 6.0) for 10 min to expose the BrdU antigen, and incubated with a 1:50 dilution of anti-BrdU antibody overnight at 4°C (Becton Dickinson, San Jose, Calif.). Biotinylated anti-mouse antibodies were used as secondary antibodies. Sections were counterstained with hematoxylin, mounted, and photographed. Cells from the embryonic, extraembryonic, and ectoplacental cones of each embryo were counted and scored for BrdU staining.

TUNEL analysis of embryos. E6.5 embryos in decidua were fixed in 4% paraformaldehyde and processed as described above. Terminal deoxynucleotidyltransferase-mediated dUTP-biotin nick end labeling (TUNEL) assays were performed on sections by using the Apoptag assay (Intergen, Purchase, N.Y.). Sections were counterstained briefly with methyl green, mounted with Permount, and photographed.

In vitro culture of E3.5 embryos. F_1 *Zfr* heterozygotes were allowed to mate for 2 h and checked for copulation plugs. E3.5 blastocysts were flushed from the uteri of plugged females and placed in gelatinized 24-well dishes. Embryos were cultured in ES cell media without the addition of leukemia inhibitory factor and then were photographed every 24 h. After 7 days in culture, the outgrowths were picked with drawn Pasteur pipettes and genotyped by PCR.

RESULTS

Targeted disruption of *Zfr* gene. To disrupt the *Zfr* gene, a targeting vector was designed in which a 6-kb region was deleted and replaced with a promoterless *lacZ*-neomycin resistance fusion gene (β*geo*) (Fig. 1A). Homologous recombination at the *Zfr* locus would result in the deletion of three exons, including the sequence encoding zinc fingers 1 and 2, disruption in the expression of the remaining downstream exons, and fusion of the *Zfr* transcription unit to β*geo*. ES cells from two homologous recombinant lines were identified and injected into C57BL/6 blastocysts (Fig. 1B and C). Chimeras were backcrossed to C57BL/6 and 129S4/SvJae mice to study the mutant phenotype on hybrid as well as pure genetic backgrounds. The phenotypes described below were consistently seen in both inbred strains and in the hybrid 129S4/SvJae × C57BL/6 mutants.

ZFR expression in early embryo. Immunolocalization experiments in the ovary had revealed that ZFR staining is strong in primary and growing oocytes (13). To determine whether maternal ZFR protein localizes to the newly formed pronuclei in the one-cell embryo, anti-ZFR immunofluorescence and 4′,6′-diamidino-2-phenylindole (DAPI) staining were performed with E0.5 embryos. Anti-ZFR staining was found in the male and the female pronucleus but not in the polar bodies (Fig. 2A). Thus, ZFR is present at the beginning of embryogenesis.

The *lacZ* gene in the targeting construct, which is under the control of the *Zfr* promoter, serves as a marker for *Zfr* expression. To determine when zygotic *Zfr* is first expressed from the paternal genome in the embryo, male mice heterozygous for the *Zfr* mutation were mated with wild-type females, and embryos were obtained at the one-cell, two-cell, four-cell, and blastocyst stages. Among 34 one-cell embryos, 25 two-cell embryos, and 20 four-cell embryos, no distinguishable X-Gal staining was observed (data not shown). Among 17 blastocysts, 5 stained well and 5 stained weakly. X-Gal stain was seen in the trophoectoderm cells as well as the inner cell mass, indicating that *Zfr* expression is not excluded from either of these primitive lineages (Fig. 2B). Thus, zygotic *Zfr* activity initiates either at the blastocyst stage or earlier at the morula stage.

The analysis of ZFR expression patterns was continued on sections of early postimplantation embryos. Anti-ZFR antibodies were used for immunohistochemical staining of normal E5.5, E6.5, and E7.5 embryos. As shown in Fig. 2C and E, ubiquitous ZFR staining was seen throughout the embryo as well as the maternal decidual tissue. ZFR staining was localized to the nucleus, but not to the nucleolus, and was absent from metaphase chromosomes (data not shown). This pattern is characteristic of the ZFR staining observed in the testis and ovary. However, whereas ZFR shows differential expression in adult mouse tissues, its expression in the early embryo is unrestricted.

Anti-ZFR immunohistochemistry performed on sections of *Zfr* homozygous mutant embryos showed immunopositive

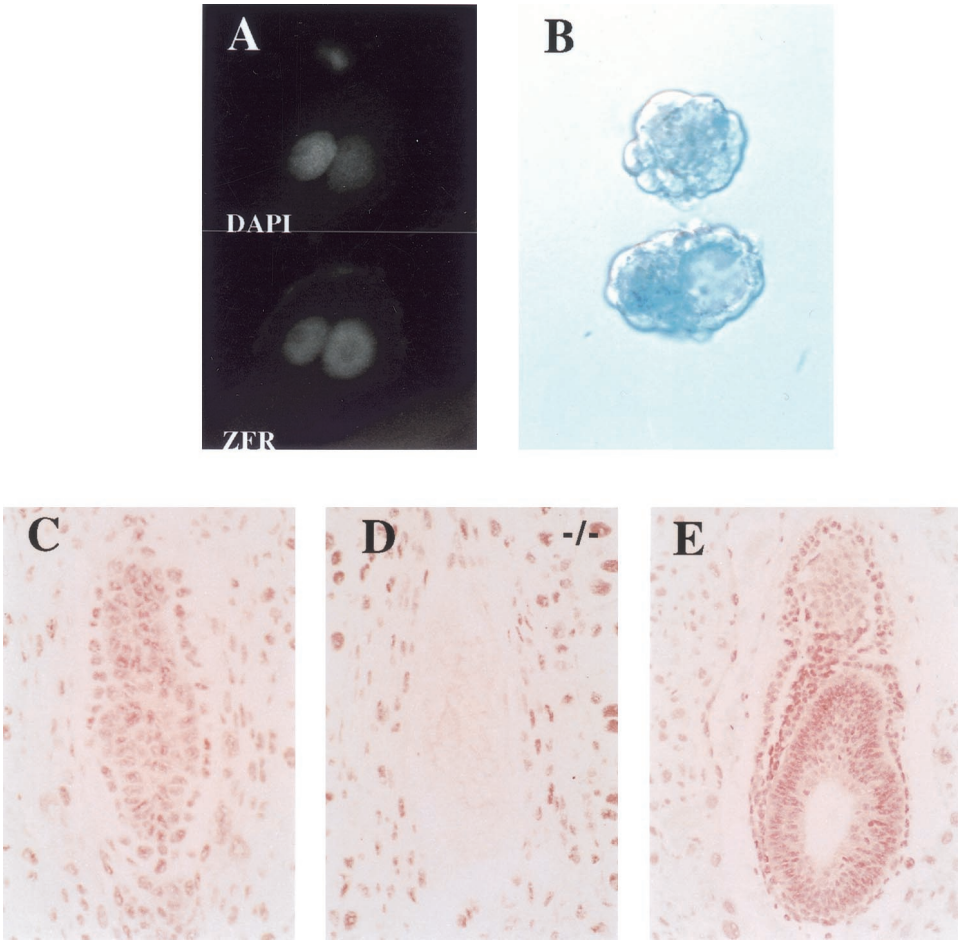

FIG. 2. Expression of ZFR in the early embryo. (A) Anti-ZFR antibody and DAPI immunofluorescence of a one-cell embryo. DAPI stains both pronuclei and the smaller polar body. Anti-ZFR staining is seen only in the pronuclei and is absent from the nucleoli. (B) X-Gal-stained E3.5 blastocysts heterozygous for the *Zfr* mutation. (C, D, E) Anti-ZFR staining of a wild-type E5.5 embryo (C), a *Zfr* homozygous mutant E5.5 embryo (D), and a wild-type E7.5 embryo (E).

staining in the heterozygous maternal decidual cells and no staining in the embryonic tissues (Fig. 2D). These observations suggest that full-length ZFR protein is not present in embryos homozygous for the targeted mutation, as predicted. Furthermore, the differential staining renders the antibodies a useful tool for genotyping sectioned embryos.

***Zfr* mutation results in early embryonic lethality.** Heterozygous *Zfr* F_1 hybrids (C57BL/6 × 129S4/SvJae) displayed no overt phenotype and were fertile. Intercrosses between heterozygotes were established to generate homozygous mutant offspring. No viable *Zfr* homozygotes were identified among the 105 born F_2 progeny, indicating that the homozygous mutation causes embryonic lethality (Table 1).

To determine the lethality profile of *Zfr* mutants, embryos from timed heterozygous intercross matings were analyzed at different days of gestation. Of the embryos dissected at E6.5, 24% were mutant in genotype, indicating that the *Zfr* mutation did not cause preimplantation lethality (Table 1). Of this class, two-thirds of the embryos appeared morphologically normal (Fig. 3A), whereas the remainder were slightly smaller than heterozygous and wild-type littermates. In general, the mutants were barely distinguishable by gross morphology at this

TABLE 1. Numbers and percentages of newborn pups and dissected E6.5, E7.5, and E8.5 embryos, classified according to phenotype and genotype

Age at dissection	No. (%) with normal phenotype and the genotype:			No. (%) with abnormal phenotype and the genotype:				Total
	+/+	+/−	−/−	+/+	+/−	−/−	Resorbed	
E6.5	18 (31)	24 (41)	9 (15)	1 (2)	0 (0)	5 (9)	1 (2)	58
E7.5	22 (26)	39 (45)	0 (0)	0 (0)	0 (0)	19 (22)	6 (8)	86
E8.5	15 (34)	18 (41)	0 (0)	0 (0)	0 (0)	8 (18)	3 (7)	44
Newborn pup	33 (31)	72 (69)	0 (0)					105

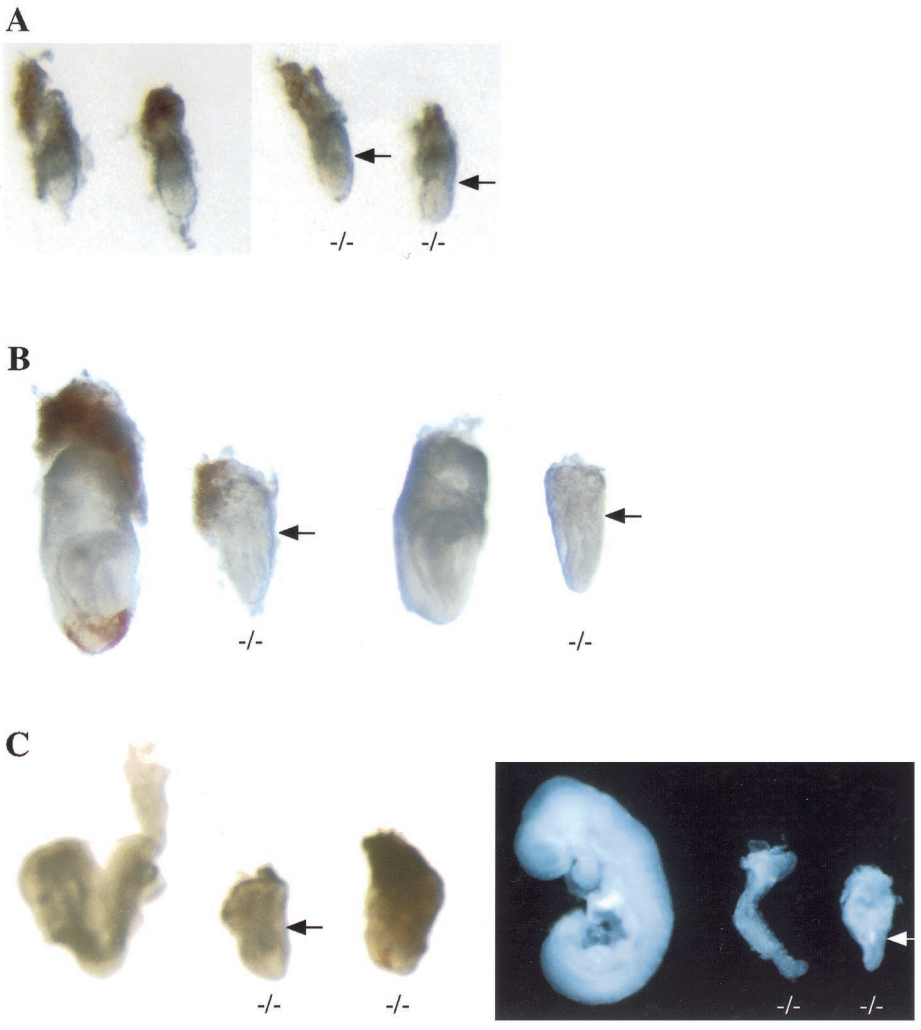

FIG. 3. Gross morphology of normal and mutant embryos from *Zfr* heterozygous intercrosses. Mutant genotypes are indicated. Arrows point to the boundary between embryonic and extraembryonic regions. (A) Two *Zfr* heterozygous E6.5 embryos (left) and two mutant littermates (right) are shown with the ectoplacental cone and Reichert's membrane. (B) A *Zfr* heterozygous E7.5 embryo and a mutant littermate shown with (left panel) and without (right panel) the ectoplacental cone and Reichert's membrane. (C, left panel) Normal (left) and mutant E8.5 embryos; (C, right panel) normal, late-stage E8.5 embryo that has completed turning, next to an advanced E8.5 *Zfr* mutant embryo with amnion removed and a degenerating *Zfr* mutant littermate.

stage. At E7.5, 22% of the embryos were homozygous mutants, and the percentage of resorbed embryos (8%) was increased. All mutants were scored as morphologically abnormal, whereas embryos with normal morphology genotyped as wild types or heterozygotes (Table 1). Mutant E7.5 embryos were found to be smaller, thinner, and developmentally retarded compared to their normal littermates (Fig. 3B). The boundary between the embryonic and extraembryonic regions could be distinguished, but both tissues were undersized. An especially narrow amniotic cavity was found to be a distinctive hallmark of the mutant phenotype.

At E8.5, all *Zfr* mutants were abnormally small (Table 1). Unlike their normal littermates, which had developed headfolds, a foregut, initial somites, and an extended allantois, *Zfr* homozygous embryos had progressed only slightly further in development (Fig. 3C, left panel). The mutant embryonic region, which was narrow at E7.5, now appeared more globular in shape and smaller than the extraembryonic region. Most mutant embryos were degenerating within sticky, necrotic extraembryonic tissue, and some embryos were starting to be resorbed. The most advanced *Zfr* mutants at this stage were grossly undersized but had developed tiny headfolds and an allantois (Fig. 3C, right panel). This observation indicates that *Zfr* mutants have the capacity to generate some of the features of a gastrulated embryo despite their impaired growth. By E10.5, resorption sites and empty decidua were found and mutant embryos were no longer recovered (data not shown). Thus, at the gross morphological level, the *Zfr* mutants manifest their phenotype between days 6.5 and 7.5 of embryonic development and die, within a short window of time, by day 9.5 or 10.5.

Histological analysis of *Zfr* homozygotes. To investigate the nature of the phenotype in greater detail, histological sections of mutant embryos from different gestation time points were stained with hematoxylin and eosin and analyzed. In general, the development and organization of the germ layers in E6.5

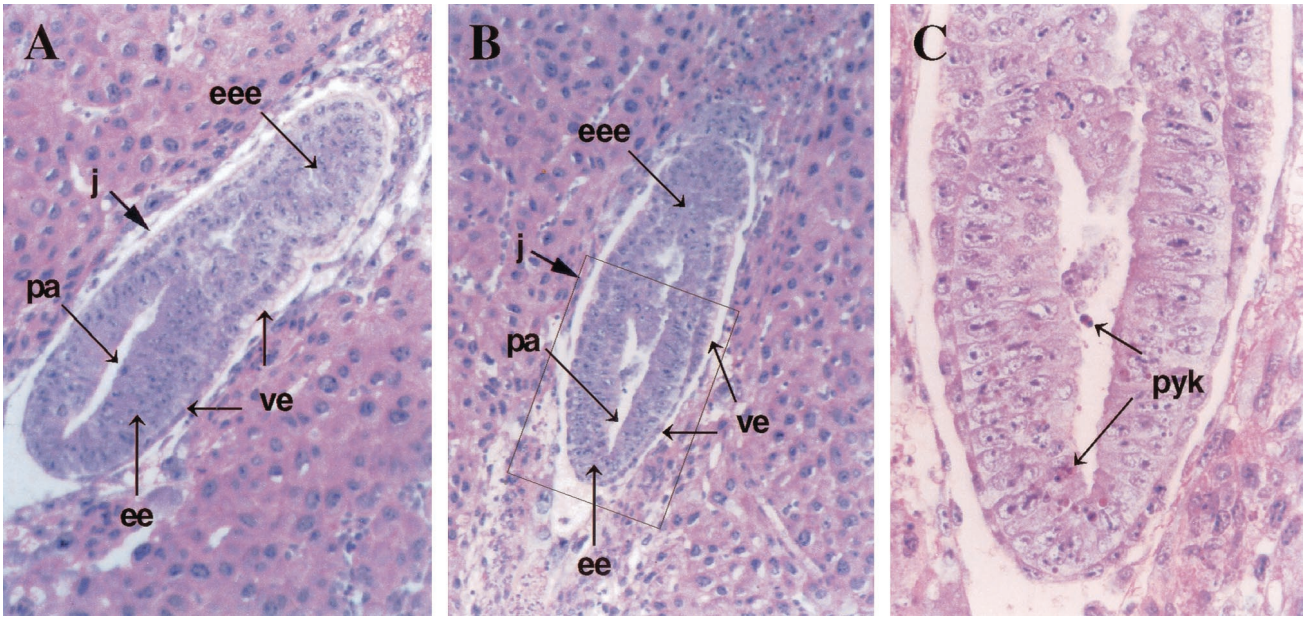

FIG. 4. Histological sections of normal (A) and *Zfr* homozygous mutant (B) E6.5 embryos stained with hematoxylin and eosin. (C) A magnified view of the distal tip of the mutant embryo, from the box in panel B. Pyknotic cells (pyk) can be observed in the embryonic ectoderm and in the proamniotic cavity (pa). eee, extraembryonic ectoderm; ee, embryonic ectoderm; ve, visceral endoderm; j, junction between embryonic and extraembryonic regions.

mutants resembled those of wild-type embryos (Fig. 4A and B). However, two deficiencies were detected in mutants at this stage. Numerous pyknotic cells were consistently found in the proamniotic cavity and in the epiblast (embryonic ectoderm) (Fig. 4C). Furthermore, the apical vacuoles in the extraembryonic endoderm cells appeared to be diminished, as greater eosin staining was observed in this region.

Sections of E7.5 embryos revealed that mutants initiate gastrulation and generate some mesodermal tissue. A normal embryo and three mutant littermates are shown in Fig. 5. The normal embryo is at the late-primitive streak stage, containing expanded amniotic and exocoelomic cavities, primitive blood islands, and primitive headfolds (Fig. 5A and B). Two mutant embryos, slightly developmentally delayed, are at the early- and mid-primitive streak stages (Fig. 5C and D). In the extraembryonic region of these mutants, posterior amniotic folds can be seen. In a third mutant, the amniotic folds have already fused to make a short amnion, a short chorion, and narrow amniotic, exocoelomic, and ectoplacental cavities (Fig. 5E). In all mutants, intraembryonic mesoderm can be seen at the primitive streak region. Extraembryonic mesoderm is apparent in the posterior amniotic folds and in the rudimentary allantois (Fig. 5E). The mutants remain smaller than the normal littermates, and pyknotic cells continue to be seen at the distal tip of the embryonic ectoderm and the amniotic cavity. Magnified photos of the columnar visceral endoderm cells from the anterior extraembryonic region of the normal embryo (Fig. 5F, the boxed region in Fig. 5A) and one of the *Zfr* mutants (Fig. 5G, the boxed region in 5E) show the paucity of apical vacuoles in the mutant cells. The microvilli present on the visceral endodermal cells appear normal in both their density and morphology (data not shown).

To better observe the organization of the three germ layers in *Zfr* mutants, a normal E7.5 embryo (Fig. 5H and J) and a *Zfr* homozygous mutant littermate (Fig. 5I and K) were sectioned transversely from the embryonic pole to the ectoplacental cone. The sections in Fig. 5H and I show a small portion, the ventral extension, of the ectoplacental cavity adjacent to the larger exocoelomic cavity. Extraembryonic mesoderm, adjacent to the extraembryonic visceral endoderm, can be seen in both the normal and *Zfr* mutant embryos. The extraembryonic region of the mutant thus has an organization similar to the normal, primitive streak stage embryo. The area of the exocoelomic cavity is nonetheless considerably smaller in the mutant. Figure 5I highlights the unusual extraembryonic visceral endoderm in the mutant. These cells, which in the normal embryo form a tight layer with discernible vacuoles at the apical ends (Fig. 5H), have a flocculent morphology and fewer apical vacuoles in the mutant embryo (Fig. 5I).

Sections through the embryo proper are shown in Fig. 5J and K. In the mutant embryo, the three germ layers are clearly evident (Fig. 5K), indicating that gastrulation has initiated. From the amnion to the embryonic pole, the embryonic pattern remains uniform. The morphology of the ectoderm suggests that its development has stalled at the advanced egg cylinder stage typical of E6.5 embryos. The transverse sections again show pyknotic cells, especially in the ectodermal layer and occasionally in the mesodermal layer. The amniotic cavity, bearing debris in most sections, is severely constricted. These observations suggest that embryonic growth is impaired in mutant embryos and that, by day 7.5, development of the embryo proper in particular is delayed with respect to extraembryonic development.

To observe the extent to which development continued within the *Zfr* embryos, mutant and wild-type E8.5 embryos were sectioned transversely and examined histologically. Fig-

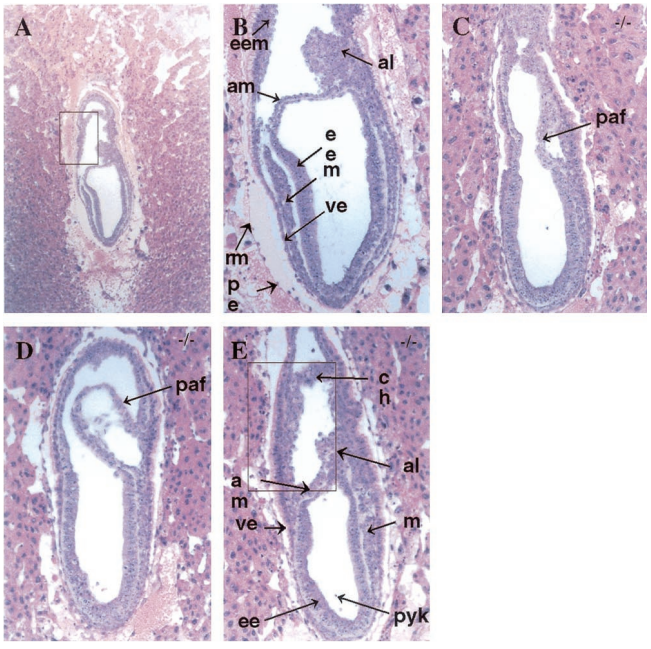

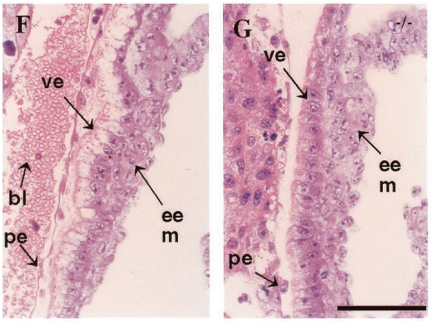

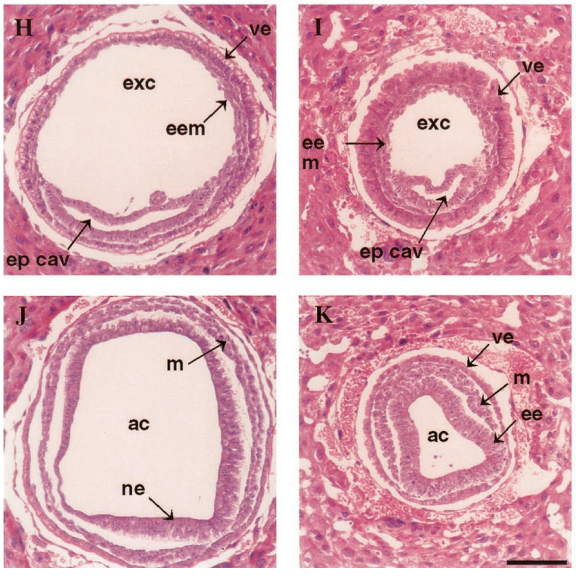

FIG. 5. Sagittal and transverse sections of normal and *Zfr* homozygous mutant E7.5 embryos. (A to E) Sagittal sections of a normal embryo (A, B) and of three *Zfr* mutant littermates (C, D, E). The posterior side of the embryo, containing the primitive streak region, is on the right in each photo. (F and G) Magnified views of the visceral endoderm at the anterior side of the normal (F) and *Zfr* mutant (G) embryos. Visceral endodermal cells have vesicles clustered at the apical side and the nucleus located at the basal side. The apical vesicles are much more apparent in the normal embryo. (H to K) Transverse sections of normal (H, J) and *Zfr* mutant (I, K) E7.5 embryos from the extraembryonic region (H, I) and from the embryonic region (J, K). al, allantois; am, amnion; eem, extraembryonic mesoderm; ee, embryonic ectoderm; m, mesoderm; ve, visceral endoderm; rm, Reichert's membrane; pe, parietal endoderm; paf, posterior amniotic fold; ch, chorion; pyk, pyknotic cell; bl, maternal blood cells; exc, exocoelomic cavity; ep cav, ectoplacental cavity; ne, neuroectoderm.

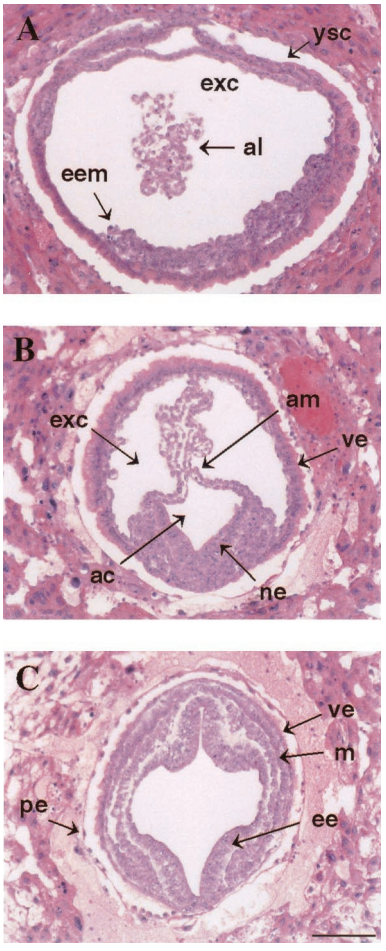

FIG. 6. Select transverse sections of an E8.5 *Zfr* mutant embryo through the extraembryonic region (A) and the embryonic region (B, C). Panel B shows the loose, disorganized amnion extending from the headfolds. ysc, yolk sac cavity; exc, exocoelomic cavity; ac, amniotic cavity; al, allantois; eem, extraembryonic mesoderm; am, amnion; pe, parietal endoderm; ve, visceral endoderm; ne, neuroectoderm; ee, embryonic ectoderm; m, mesoderm.

ure 6 shows mutant embryo sections through the extraembryonic region (Fig. 6A), the headfolds (Fig. 6B), and through the distal portion of the embryo (Fig. 6C). The chorion and exocoelomic cavity has expanded since the E7.5 stage, and within the cavity the allantois and accumulated extraembryonic me-

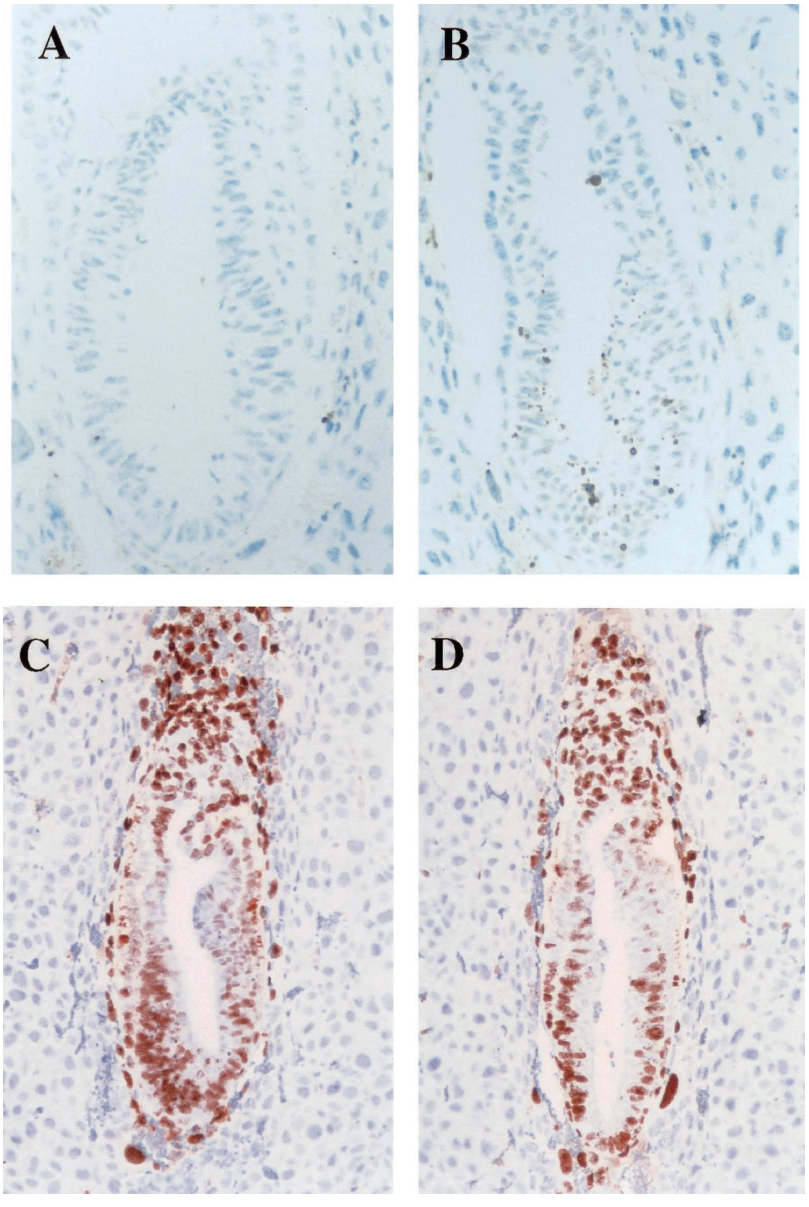

FIG. 7. TUNEL assay (A, B) and anti-BrdU immunohistochemistry (C, D) with sections of normal (A, C) and *Zfr* homozygous mutant (B, D) E6.5 embryos. (A, B) The brown precipitate (3,3′-diaminobenzidine) shows antidigoxigenin antibody staining of digoxigenin-dUTP that had been incorporated at fragmented DNA ends by terminal transferase. Sections are counterstained with methyl green. (C, D) The red stain indicates BrdU-positive, proliferating cells. Sections are counterstained with hematoxylin.

soderm are observed (Fig. 6A). In the embryonic region, adjacent to small headfolds, is an abnormal amnion. Composed of a layer of embryonic ectodermal cells plus a layer of extraembryonic mesodermal cells, the amnion is normally a thin, taut tissue covering the amniotic cavity. The developing headfolds push up against the amnion, such that the amnion stretches over the headfolds laterally and along the anterior-posterior axis (7). In *Zfr* mutants, the amnion is loose, disorganized, and involuted to the point of sharply compressing part of the amniotic cavity (Fig. 6B). Development of the embryo proper is severely delayed. The structures typical of the E8.5 stage are not apparent except for the presence of abnormal-appearing neuroectodermal folds (Fig. 6C). The morphology of the E8.5 *Zfr* mutant embryo shows a general failure in growth, tissue differentiation, and body plan organization. These results correlate with the observations noted from dissections of advanced E8.5 *Zfr* mutants.

Increased cell death in ectoderm of *Zfr* mutant embryos. Pyknotic cells were commonly observed in histological sections of *Zfr* mutant embryos. Especially prominent in the embryonic ectoderm, these abnormal cells were often the first indication of the mutant genotype at E6.5. To determine whether the frequent pyknosis and growth failure of *Zfr* mutant embryos were associated with increased programmed cell death, a TUNEL assay was performed on sections of E6.5 embryos.

The TUNEL assay was performed on sagittal sections near

the midline of 7 *Zfr* mutants and 22 normal E6.5 embryos (Fig. 7A and B). Apoptotic cells were expected to be observed in sections of *Zfr* wild-type and heterozygous embryos, as programmed cell death naturally occurs during early embryogenesis (11). Among the normal embryo sections, an average of 13.2 TUNEL-positive cells per section were counted. In contrast, mutant embryos displayed a prominent and statistically significant increase in the number of TUNEL-positive cells, averaging 43.7 TUNEL-positive cells per section (Student's *t* test, $P < 0.0005$). The apoptotic bodies were especially common in the embryonic ectoderm tissue and were often clustered near the distal end of the mutant embryos (Fig. 7B).

Decreased proliferation rates in *Zfr* mutant embryos. A second possibility that could contribute to the small size and narrow cavities in *Zfr* homozygous mutant embryos is a defect in embryonic cell proliferation. To examine the mitotic index of the *Zfr* mutants, pregnant females from *Zfr* heterozygote intercrosses carrying E6.5 embryos were injected with BrdU 1 h prior to dissection. Sections of embryos in decidual swellings were processed for anti-BrdU immunohistochemistry. Sagittal sections close to the midline of five mutant and four normal embryos were selected and examined (Fig. 7C and D). BrdU-positive and -negative cells were counted and classified as belonging to the embryonic, extraembryonic, or ectoplacental region. Calculation of the number of BrdU-positive cells divided by the total number of cells generated the mitotic index value. When cells from all regions of the embryos were counted, an average mitotic index of 0.78 was found for the normal class of embryos. A significantly lower average mitotic index of 0.69 was found for the mutant embryos (Student's *t* test, $P < 0.025$).

In transverse sections of E7.5 *Zfr* mutants, a more pronounced developmental delay was observed in the embryo proper versus the extraembryonic region. Similarly, the TUNEL assay showed localized programmed cell death in the embryonic ectoderm. It therefore was possible that, in mutant embryos, proliferation rates in embryonic tissues were more severely affected than those in extraembryonic tissues. When calculated for the embryonic regions exclusively, the average mitotic indices were 0.76 for normal embryos and 0.61 for mutant embryos (Student's *t* test, $P < 0.005$). In contrast, the average mitotic index for the combined extraembryonic and ectoplacental regions was 0.76 for normal embryos and 0.73 for mutant embryos. The fraction of BrdU incorporation in mutants was therefore especially low in the embryo proper but not significantly different in the extraembryonic tissues.

The *Zfr* mutation causes degeneration of in vitro-cultured blastocyst outgrowths. To assay the intrinsic growth and survival potential of the *Zfr* mutant embryos, E3.5 embryos obtained from timed *Zfr* heterozygous intercross matings were cultured in vitro for 7 days. Grown in ES cell media without supplemental LIF, the blastocyst outgrowths were monitored daily and ultimately genotyped by PCR on the last day. Eleven *Zfr* heterozygous, five *Zfr* homozygous, and six wild-type embryos were assayed. As blastocysts, the *Zfr* mutants displayed no overt anomalies, suggesting that the *Zfr* mutation does not lead to a preimplantation phenotype. All of the blastocysts successfully attached to the culture dish, hatched from the zona pellucida, and initiated growth. Proliferating and differentiating inner cell masses, surrounded by trophoblasts, were observed in wild-type and *Zfr* heterozygous outgrowths. Cavitation of the inner cell mass was observed by the seventh day of culture for 10 of the 17 wild types and heterozygotes.

Outgrowths from four *Zfr* homozygous mutant blastocysts grew aberrantly in culture. Initially, mutant blastocyst outgrowths were indistinguishable from the remaining outgrowths. Comparable growth of the inner cell mass and trophoblasts could be seen in a wild-type and in a mutant blastocyst after 2 and 4 days in culture (Fig. 8). Shortly thereafter, by day 5, obviously undersized inner cell masses were observed in the four mutants. In three cases, the inner cell mass subsequently deteriorated, leaving mostly trophoblast cells behind (Fig. 8). The fourth mutant outgrowth did not degenerate and instead grew slightly through day 7 despite its reduced size. These observations thus confirm that the *Zfr* mutation can detrimentally affect the growth of blastocysts when cultured outside the maternal environment. The impaired growth of the mutant embryos could be a manifestation of increased programmed cell death, decreased cellular proliferation, or both. Among the *Zfr* mutant blastocysts, one exception to the course of development described above was found. A fifth mutant outgrowth grew as well as the normal embryos and developed a substantial, differentiated, but not cavitated, inner cell mass by day 7.

Analysis of *Zfr*-deficient embryos in *Trp53* null background. The tumor suppressor gene *Trp53* (encoding p53) plays a central role in the control of apoptosis and cell cycle progression. To determine whether the phenotype seen in *Zfr* mutant embryos would be altered by the loss of p53 function, *Zfr* heterozygous females were mated to *Trp53* heterozygous males to obtain compound heterozygotes. The $Zfr^{+/-}$ $Trp53^{+/-}$ animals were intercrossed, and litters were dissected at E8.5. The rationale for choosing this time point was based on the *Zfr* phenotype and results from genetic crosses of *Trp53* with other mutations. A *Trp53*-deficient genetic background was found to partially rescue the developmental life span of embryos deficient for *Brca1, Brca2, Rad51*, or *Xrcc1*, presumably because cell cycle checkpoints, apoptosis, or both pathways, were no longer activated (9, 10, 20). At E8.5, the *Zfr* null embryos could still be dissected and accurately genotyped but were tiny and deformed. Thus, any rescue of the *Zfr* phenotype by the *Trp53* mutation would most likely be morphologically distinct at this stage. Among 126 embryos dissected, only one $Zfr^{-/-}$ $Trp53^{-/-}$ double mutant embryo was isolated, strongly suggesting that loss of p53 in *Zfr* mutants does not rescue the *Zfr* embryos from demise at E8.5.

DISCUSSION

The *Zfr* mutation results in embryonic cell death, growth impairment, and dysmorphogenesis. Elimination of the *Zfr* gene has severe consequences for postimplantation and gastrulation stage development. Early indications of embryonic failure can be detected prior to primitive streak formation at E6.5. At this stage, *Zfr* mutants display increased cell death in the epiblast and decreased vacuolization in the visceral endoderm. Cellular proliferation slows, and consequently, primitive streak embryos are growth retarded. As gastrulation proceeds, a loose amnion develops to cover the constricted amniotic cavity. At their most advanced state, the tiny headfold-stage *Zfr* mutants are morphologically anomalous and are

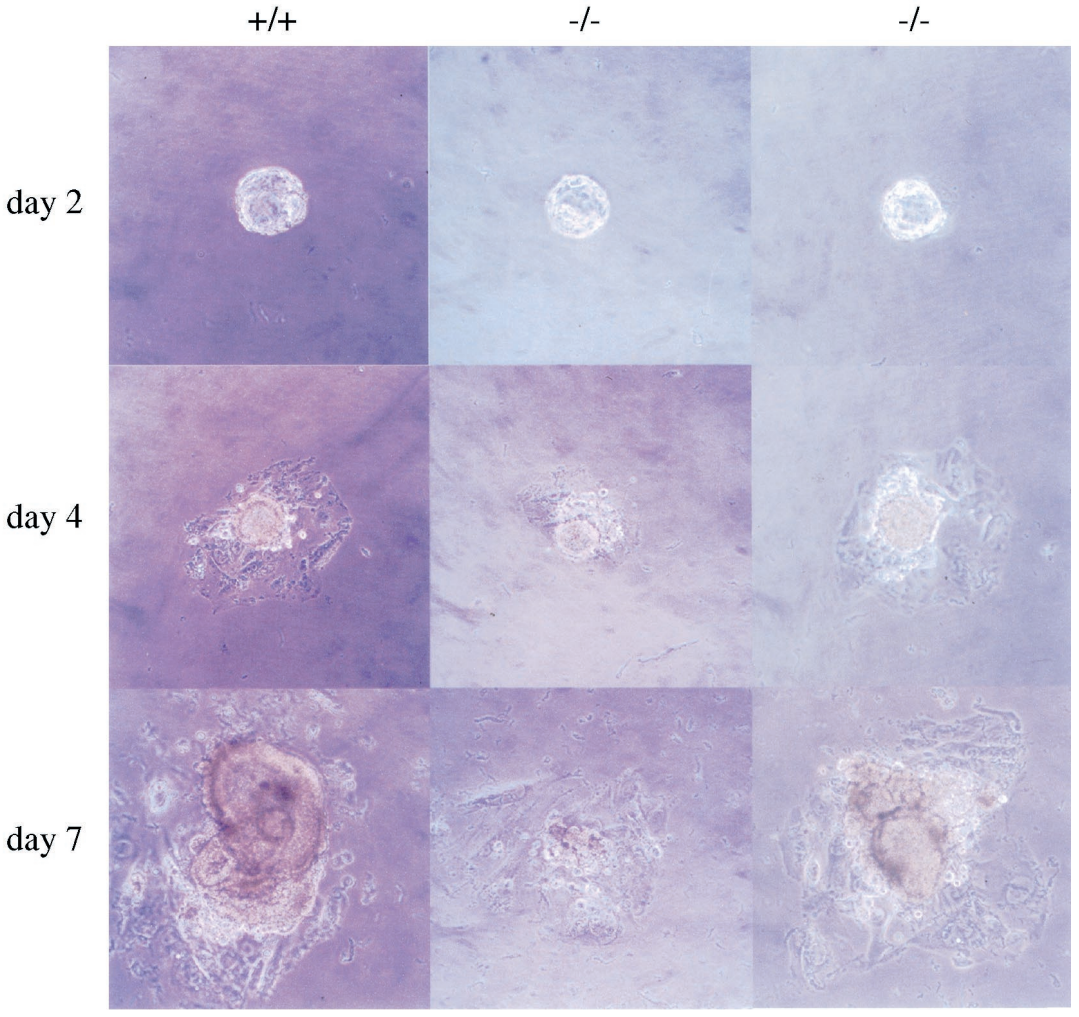

FIG. 8. In vitro culture of wild-type (left) and *Zfr* homozygous mutant (middle and right) blastocysts, photographed after 2, 4, or 7 days of culture. Trophoblast cells can be seen surrounding the inner cell mass outgrowths.

degenerating. The embryonic tissues appear to be particularly blighted in comparison with the extraembryonic region, which exhibits a grossly normal chorion and allantois. Despite the growth deficiency and abnormal levels of programmed cell death at E6.5, *Zfr* mutants are not impaired in primitive streak formation and mesoderm differentiation and migration. Extraembryonic mesodermal structures, including proamniotic folds, chorion, and allantois, develop, and attachment of the allantois to the chorion was observed. Thus, the *Zfr* mutation is distinct from mutations that interrupt the gastrulation process directly.

The visceral endoderm, an extraembryonic tissue, serves a number of functions critical for the proper development of the conceptus. In addition to its role in developmental patterning of the underlying ectodermal tissue (2), the visceral endoderm cells supply nutrients to the embryonic tissue by synthesizing serum components and endocytosing maternal macromolecules that have passed through Reichert's membrane into the parietal yolk sac cavity (3). The columnar visceral endoderm cells adjacent to the extraembryonic ectoderm are specialized for this task; polarized in organization, these cells contain many lysosomes and microvilli at the apical surface. The anomalous morphology noted in the *Zfr* visceral endoderm cells could be an indication of a requirement for ZFR in visceral endoderm function. One possible interpretation of the *Zfr* phenotype is that some of the nutritional links between the visceral endoderm and the adjacent ectoderm are disrupted, which in turn leads to survival and proliferation problems in the embryonic ectoderm. The combination of ectodermal cell death and anomalous visceral endoderm histology at gastrulation stages has been described with other mouse mutants, notably the *huntingtin* and *hnf4* mutants (4, 21).

At the start of gastrulation at E6.5, *Zfr* mutants display increased apoptosis in the embryonic ectoderm and decreased cell proliferation rates in vivo. When cultured in vitro, most E3.5 mutant embryos degenerate by 7 days of culture. Wild-type and *Zfr* heterozygote outgrowths, by comparison, show continual growth of the inner cell mass. The compromised growth of the *Zfr* mutant embryonic cells in vivo and in vitro suggests the hypothesis that the embryonic cells are intrinsically impaired by the *Zfr* mutation. The *Zfr* phenotype becomes more apparent when the embryonic growth rate in-

creases and the length of the cell cycle decreases. These changes at gastrulation could be responsible for the developmental course observed in *Zfr* mutants. However, in an investigation of four genes involved in cell cycle control and DNA surveillance, *Brca1, p21, p53*, and *mdm2* showed no difference in expression among wild-type, heterozygous, and mutant E6.5 littermate embryos (unpublished data).

Making it to gastrulation: possibilities for cell lethality and maternal rescue in *Zfr* embryos. Experiments to address the tissue distribution of *Zfr* transcripts revealed that *Zfr* is most highly expressed in the testis, brain, and ovary, suggesting that ZFR has an important activity in the function or development of cells in these tissues (13). The low-level expression of *Zfr* in other tissues as well pointed to the possibility that *Zfr* is expressed in a variety of cells at modulated levels. Our first observation of ZFR expression during embryogenesis came from investigating whether the ZFR expression in oocyte nuclei was continued in the one-cell embryo. The observed localization of ZFR in the male and female pronuclei and the detection of β-galactosidase expressed from the targeted *Zfr* allele in blastocysts suggested that *Zfr* might be essential for preimplantation development.

An embryo reaching the gastrulation stage of early embryogenesis has already succeeded in several fundamental events. *Zfr*-deficient embryos are capable of undergoing cell division, cell differentiation, and ingression into the uterine tissue. The ability of the mutant embryos to pass these critical phases suggests that the *Zfr* gene product is not required initially in development. Alternatively, *Zfr* may be required in an autonomous fashion by all cells throughout the early stages of embryogenesis, including the pre- and perigastrulation stages. In the absence of zygotic *Zfr*, the early $Zfr^{-/-}$ embryo might be accumulating subtle damage that only later leads to an observable phenotype, as has been hypothesized for the DNA repair and tumor suppressor mutants described earlier. A second factor that could permit the survival of *Zfr* mutant embryos to gastrulation is rescue by maternal *Zfr* RNA or protein present in one-cell embryos. Maternal gene products are generally not considered to play an important role in mouse embryonic development beyond the two-cell stage, at which time the zygotic genome becomes activated. Coincident with this activation, specific degradation of maternal RNAs and rapid turnover of proteins encoded by maternal messages have been observed (5, 7). However, reports of targeted mutations in the mitochondrial oxidative gene *Dld* and cyclin A2 gene have nevertheless invoked the possibility of maternal rescue prolonging the lifespan of the mutants (8). It is possible that small amounts of maternal ZFR protein are retained beyond implantation and permit development to proceed to gastrulation.

ACKNOWLEDGMENTS

We thank Phil Soriano for many helpful discussions and for the generous gift of the AK47 ES cells, Kathy Kafer for expert technical assistance, and Bill Buaas for many critical discussions and advice.

This work was supported by a grant from NICHD (HD12629) through a cooperative agreement as part of the Specialized Cooperative Centers Program in Reproduction Research.

REFERENCES

1. **Bancroft, J. D., and A. Stevens.** 1996. Theory and practice of histological techniques, 4th ed. Churchill Livingstone, New York, N.Y.
2. **Beddington, R. S., and E. J. Robertson.** 1998. Anterior patterning in mouse. Trends Genet. **14:**277–284.
3. **Bielinska, M., N. Narita, and D. B. Wilson.** 1999. Distinct roles for visceral endoderm during embryonic mouse development. Int. J. Dev. Biol. **43:**183–205.
4. **Duyao, M. P., A. B. Auerbach, A. Ryan, F. Persichetti, G. T. Barnes, S. M. McNeil, P. Ge, J. P. Vonsattel, J. F. Gusella, A. L. Joyner, et al.** 1995. Inactivation of the mouse Huntington's disease gene homolog Hdh. Science **269:**407–410.
5. **Flach, G., M. H. Johnson, P. R. Braude, R. A. Taylor, and V. N. Bolton.** 1982. The transition from maternal to embryonic control in the 2-cell mouse embryo. EMBO J. **1:**681–686.
6. **Hakem, R., J. L. de la Pompa, C. Sirard, R. Mo, M. Woo, A. Hakem, A. Wakeham, J. Potter, A. Reitmair, F. Billia, E. Firpo, C. C. Hui, J. Roberts, J. Rossant, and T. W. Mak.** 1996. The tumor suppressor gene Brca1 is required for embryonic cellular proliferation in the mouse. Cell **85:**1009–1023.
7. **Hogan, B., R. Beddington, F. Constantini, and E. Lacy.** 1994. Manipulating the mouse embryo, 2nd ed. Cold Spring Harbor Laboratory Press, Cold Spring Harbor, N.Y.
8. **Johnson, M. T., H. S. Yang, T. Magnuson, and M. S. Patel.** 1997. Targeted disruption of the murine dihydrolipoamide dehydrogenase gene (Dld) results in perigastrulation lethality. Proc. Natl. Acad. Sci. USA **94:**14512–14517.
9. **Lim, D. S., and P. Hasty.** 1996. A mutation in mouse *rad51* results in an early embryonic lethal that is suppressed by a mutation in *p53*. Mol. Cell. Biol. **16:**7133–7143.
10. **Ludwig, T., D. L. Chapman, V. E. Papaioannou, and A. Efstratiadis.** 1997. Targeted mutations of breast cancer susceptibility gene homologs in mice: lethal phenotypes of Brca1, Brca2, Brca1/Brca2, Brca1/p53, and Brca2/p53 nullizygous embryos. Genes Dev. **11:**1226–1241.
11. **Manova, K., C. Tomihara-Newberger, S. Wang, A. Godelman, S. Kalantry, K. Witty-Blease, V. De Leon, W. S. Chen, E. Lacy, and R. F. Bachvarova.** 1998. Apoptosis in mouse embryos: elevated levels in pregastrulae and in the distal anterior region of gastrulae of normal and mutant mice. Dev. Dyn. **213:**293–308.
12. **Matsui, M., M. Oshima, H. Oshima, K. Takaku, T. Maruyama, J. Yodoi, and M. M. Taketo.** 1996. Early embryonic lethality caused by targeted disruption of the mouse thioredoxin gene. Dev. Biol. **178:**179–185.
13. **Meagher, M. J., J. M. Schumacher, K. Lee, R. W. Holdcraft, S. Edelhoff, C. Disteche, and R. E. Braun.** 1999. Identification of ZFR, an ancient and highly conserved murine chromosome-associated zinc finger protein. Gene **228:**197–211.
14. **Ramirez-Solis, R., A. C. Davis, and A. Bradley.** 1993. Gene targeting in embryonic stem cells. Methods Enzymol. **225:**855–878.
15. **Rowinski, J., D. Solter, and H. Koprowski.** 1975. Mouse embryo development in vitro: effects of inhibitors of RNA and protein synthesis on blastocyst and post-blastocyst embryos. J. Exp. Zool. **192:**133–142.
16. **Sambrook, J., E. F. Fritsch, and T. Maniatis.** 1989. Molecular cloning: a laboratory manual, 2nd ed. Cold Spring Harbor Laboratory Press, Cold Spring Harbor, N.Y.
17. **Sharan, S. K., M. Morimatsu, U. Albrecht, D. S. Lim, E. Regel, C. Dinh, A. Sands, G. Eichele, P. Hasty, and A. Bradley.** 1997. Embryonic lethality and radiation hypersensitivity mediated by Rad51 in mice lacking Brca2. Nature **386:**804–810.
18. **Snow, M. H.** 1977. Gastrulation in the mouse: growth and regionalization of the epiblast. J. Embryol. Exp. Morphol. **42:**293–303.
19. **Suzuki, A., J. L. de la Pompa, R. Hakem, A. Elia, R. Yoshida, R. Mo, H. Nishina, T. Chuang, A. Wakeham, A. Itie, W. Koo, P. Billia, A. Ho, M. Fukumoto, C. C. Hui, and T. W. Mak.** 1997. Brca2 is required for embryonic cellular proliferation in the mouse. Genes Dev. **11:**1242–1252.
20. **Tebbs, R. S., M. L. Flannery, J. J. Meneses, A. Hartmann, J. D. Tucker, L. H. Thompson, J. E. Cleaver, and R. A. Pedersen.** 1999. Requirement for the Xrcc1 DNA base excision repair gene during early mouse development. Dev. Biol. **208:**513–529.
21. **Zeitlin, S., J. P. Liu, D. L. Chapman, V. E. Papaioannou, and A. Efstratiadis.** 1995. Increased apoptosis and early embryonic lethality in mice nullizygous for the Huntington's disease gene homologue. Nat. Genet. **11:**155–163.